Applied Physics Letters

Analysis of edge threading dislocations $\vec{b} = \frac{1}{2}\langle 110 \rangle$ in three dimensional Ge crystals grown on (001)-Si substrates

Cite as: Appl. Phys. Lett. **107**, 093501 (2015); https://doi.org/10.1063/1.4929422
Submitted: 18 June 2015 . Accepted: 06 August 2015 . Published Online: 31 August 2015

Y. Arroyo Rojas Dasilva, M. D. Rossell, D. Keller, P. Gröning, F. Isa, T. Kreiliger, H. von Känel, G. Isella, and R. Erni

Analysis of edge threading dislocations $\vec{b}=\frac{1}{2}\langle 110\rangle$ in three dimensional Ge crystals grown on (001)-Si substrates

Y. Arroyo Rojas Dasilva,[1,a)] M. D. Rossell,[1] D. Keller,[1,2] P. Gröning,[3] F. Isa,[4] T. Kreiliger,[4] H. von Känel,[4] G. Isella,[5] and R. Erni[1]
[1]*Electron Microscopy Center, EMPA, Swiss Federal Laboratories for Materials Science and Technology, Dübendorf, Switzerland*
[2]*Laboratory for Thin Films and Photovoltaics, EMPA, Swiss Federal Laboratories for Materials Science and Technology, Dübendorf, Switzerland*
[3]*Advanced Materials and Surfaces, EMPA, Swiss Federal Laboratories for Materials Science and Technology, Dübendorf, Switzerland*
[4]*Solid State Physics Laboratory, ETH, Zurich, Switzerland*
[5]*L-NESS and Department of Physics, Politecnico di Milano, Como, Italy*

(Received 18 June 2015; accepted 6 August 2015; published online 31 August 2015)

Threading dislocations (TDs) in germanium (Ge) crystals epitaxially grown on a patterned (001)-silicon (Si) substrate are investigated using transmission electron microscopy (TEM) techniques. Analysis of dislocations performed on the Ge crystals reveals 60° and edge TDs with Burgers vector $\vec{b}=\frac{1}{2}\langle 110\rangle$. High-angle annular dark-field scanning TEM (HAADF-STEM) is used to observe the core of the edge TDs at atomic scale. Pairs of TDs with $\vec{b}=\frac{1}{2}\langle 110\rangle$ are present in the material running parallel at small distances between them (0.5–1.5 nm). The observation of such parallel dislocation pairs in Ge has not been documented before. The interaction between the edge dislocation pairs is obtained experimentally from the high-resolution HAADF-STEM images by applying geometrical phase analysis. The experimental strain maps are compared to analytical calculations based on the anisotropic elastic theory demonstrating a good match between them. [http://dx.doi.org/10.1063/1.4929422]

Dislocations are the most common defect found in epitaxial heterostructures due to the lattice and thermal mismatches between the epitaxial layer and the substrate. Threading dislocations (TDs) are the major source of defects in heterostructures affecting the performance of devices such as solar cells, light emitting diodes, transistors, and photodetectors.[1] Epitaxial Ge/Si heterostructures have been extensively studied due to their excellent optoelectronic properties.[2] The Ge/Si system is, however, characterized by a large lattice mismatch of 4.2% and contains a large threading dislocation density ($>10^8\,\mathrm{cm}^{-2}$).[3] These dislocations affect the optoelectronic properties of the devices due to the elastic distortions around the line direction causing deformation in the crystal lattice[4] and acting as recombination-regeneration centers.[5] The onset of the plastic strain relaxation in out-of-equilibrium growth of Ge on (001)-Si has recently been shown to be governed mainly by 60° misfit dislocations (MDs) spaced by atomic distances, while 90° MDs appear to be in minority.[6] 60° TDs with Burgers vector $\vec{b}=\frac{1}{2}\langle 110\rangle$ lying on {111} planes and TDs along the [001] direction have also been found in 3-dimensional (3D) epitaxial Ge crystals.[7–9] The TDs along the [001] direction have been identified to have screw and edge character with Burgers vectors $\vec{b}=\langle 001\rangle$ and $\vec{b}=\frac{1}{2}\langle 110\rangle$, respectively. Several methods have been used to reduce the threading dislocation density[9,10] in 3D Ge crystals in order to improve their properties. Additionally, the strain fields around dislocations in Ge films have been simulated with different dislocations models, such as isotropic[11,12] and anisotropic elastic theory,[12] and Peierls-Nabarro and Foreman models, and compared with the experimental results. For example, the Peierls-Nabarro model was used to describe edge core dislocations in Au[12] and Ge,[13] and the Foreman model in α-Fe_2O_3/α-Al_2O_3[14] and Ge/Si.[15]

In the present work, a detailed TDs analysis was performed on Ge crystals grown on Si patterned substrates using transmission electron microscopy (TEM) techniques. Atomic resolution images (high-angle annular dark-field scanning TEM (HAADF-STEM)) were used to obtain the experimental strain fields of two different pairs of parallel threading dislocations using geometrical phase analysis (GPA). Simulation of the strain fields was carried out using the anisotropic elastic theory and compared to the experimental data.

The Ge crystals were grown on (001)-Si substrates patterned in the form of tall pillars by Low Energy Plasma Enhanced Chemical Vapor Deposition (LEPECVD) with growth temperature and rate of 550 °C and 4.2 nm/s, respectively.[10] The dimensions of the Si pillars were 5×5 and $15\times 15\,\mu\mathrm{m}^2$ with Ge heights ranging between 8 and 30 μm, respectively. Figure 1 shows a scanning electron microscopy (SEM) image of the Ge crystals grown along the [001] direction on a patterned Si substrate. The central part of the top surface consists of the (001) facet, and close to the borders {113} and {111} facets are formed.[10] TEM cross sectional samples were prepared by mechanical polishing, dimple grinding, and ion milling using a Fishione ion miller model 1050 at 3 kV (Ar) to achieve electron transparency. Plan-view samples for the HAADF-STEM analysis were prepared using a focus ion beam (FEI Helios NanoLab 600i DualBeam). The analysis of the dislocations was carried out

a)Yadira.Arroyo@empa.ch

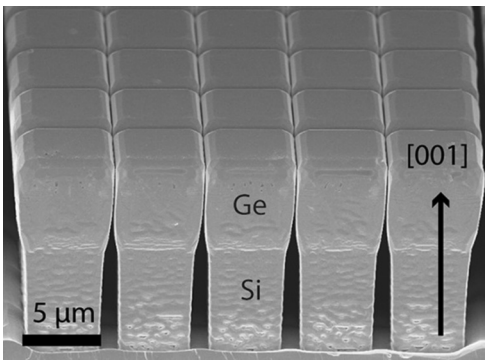

FIG. 1. SEM image of the 8 μm tall Ge crystals on top of $5 \times 5\ \mu m^2$ Si pillars.

using a Philips CM 30 microscope at 300 kV, and the identification was performed using $\vec{g}.\vec{b} = 0$ (invisibility criterion) and two beams condition. The HAADF-STEM analysis was performed using a double spherical aberration-corrected JEOL JEM-ARM200F microscope operated at 200 kV. The microscope was set up in STEM mode with a probe semiconvergent angle 25.3 mrad and the annular semidetection range of the annular dark-field (DF) detector was calibrated at 68–280 mrad.

GPA[16] is commonly applied to determine the local displacement and strain fields around the dislocation cores from atomic scale images. HRTEM[12,17] and HAAD-STEM[11] images were previously used to obtain displacement and strain field maps. The artifacts related to thickness and defocus effects in HRTEM are avoided by using High resolution STEM (HRSTEM). However, STEM images often suffer from distortions due to the line to line scanning errors which can impact the analysis. Recently, strain field studies in Ge have been reported for single dislocations,[18,19] but not for two parallel dislocation close to each other.

Simulations were performed using the pure straight edge dislocations in the anisotropic media theory. The coordinate system x_1, x_2, and x_3 for a cubic crystal is given for the crystallographic directions [100], [010], and [001], and the elastic constants c_{ij} for the Ge are $c_{11} = 128.9$ GPa, $c_{12} = 48.3$ GPa, and $c_{44} = 67.1$ GPa.[20] For the calculations, the dislocation line was aligned parallel to the x_3 axis and the x_1, x_2 axes were rotated 45°; the transformed coordinate system x'_1, x'_2, and $x'_3 = x_3$ are $[1\bar{1}0]$, [110], and [001] directions, respectively. The transformed elastic constants c'_{ij} for the transformed coordinate system are $c'_{11} = c'_{22} = 155.7$ GPa, $c'_{12} = 21.5$ GPa, and $c'_{66} = 40.3$ GPa. The magnitude of the Burgers vector is similar for all the dislocations, $a/\sqrt{2}$, where a is the lattice parameter 0.5689 nm. The anisotropic theory describes the displacement of the edge dislocations with Burgers vector $\vec{b} = (b_x, b_y, 0)$[20] as

$$u_x = -\frac{b_x}{4\pi}\left(\arctan\frac{2xy\lambda\sin\phi}{x^2-\lambda^2y^2} + \frac{\bar{c}'^2_{11}-c'^2_{12}}{2\bar{c}'_{11}c'_{66}\sin 2\phi}\ln\frac{q}{t}\right) - \frac{b_y}{4\pi\lambda\bar{c}'_{11}\sin 2\phi}\left[(\bar{c}'_{11}-c'_{12})\cos\phi\ln qt - (\bar{c}'_{11}+c'_{12})\sin\phi\arctan\frac{x^2\sin 2\phi}{\lambda^2y^2-x^2\cos 2\phi}\right], \quad (1)$$

$$u_y = \frac{\lambda b_x}{4\pi\bar{c}'_{11}\sin 2\phi}\left[(\bar{c}'_{11}-c'_{12})\cos\phi\ln qt - (\bar{c}'_{11}+c'_{12})\sin\phi\arctan\frac{y^2\lambda^2\sin 2\phi}{x^2-\lambda^2y^2\cos 2\phi}\right] - \frac{b_y}{4\pi}\left(\arctan\frac{2xy\lambda\sin\phi}{x^2-\lambda^2y^2} + \frac{\bar{c}'^2_{11}-c'^2_{12}}{2\bar{c}'_{11}c'_{66}\sin 2\phi}\ln\frac{q}{t}\right), \quad (2)$$

where $q^2 = x^2 + 2xy\lambda\cos\phi + y^2\lambda^2$, $t^2 = x^2 - 2xy\lambda\cos\phi + y^2\lambda^2$, $\lambda = \left(\frac{c'_{11}}{c'_{22}}\right)^{1/4}$, $\phi = \frac{1}{2}\arccos\frac{c'^2_{12}+2c'_{12}c'_{66}-\bar{c}'^2_{11}}{2c'_{11}c'_{66}}$.

Figure 2(a) shows a DF image of the top of a Ge crystal under $\vec{g} = (2\bar{2}0)$ diffraction condition. The analysis of the dislocations shows that the majority of the dislocations are 60° TDs with $\vec{b} = \frac{1}{2}\langle 110\rangle$ lying on {111} planes. Since the {111} planes are inclined 54.73° from the {001} planes, these dislocations are ending at the sidewalls of the crystals. TDs along the [001] line direction (black arrows in Figure 2(a)) have been also observed in the Ge crystals with $\vec{b} = \frac{1}{2}[1\bar{1}0]$ and $\vec{b} = [001]$. They have edge and screw character, respectively. The density of the edge TDs is much higher than that of the screw TDs (up to 9:1). These edge TDs end at the top surface or bend to the sidewalls in the Ge crystals. They are created by a change of direction of a dislocation loop or by 60° TD, as shown in Figure 2(b), where the dislocations 1 and 2 are edge TDs with $\vec{b} = \frac{1}{2}[1\bar{1}0]$. Dislocations 3 and 4 from Figure 2(b), with $\vec{b} = \frac{1}{2}[101]$ (3) and $\vec{b} = \frac{1}{2}[01\bar{1}]$ (4), cannot interact with each other and form the TD1 because there is no reduction of energy ($\frac{1}{2}[101] + \frac{1}{2}[01\bar{1}] \rightarrow [110]$, $a^2 \rightarrow 2a^2$). Therefore, one of the dislocations appears to change direction and form the edge TDs (1). For the TD2, the dislocation loop (5) changes direction whereby TD2 is formed. TD2 and TD5 have both the same $\vec{b} = \frac{1}{2}[1\bar{1}0]$. The reason for their formation and the impact on the physical properties of the Ge pillars are subject of future investigations.

The TDs along the [001] line direction are also analyzed by HAADF-STEM in the [001] zone axis. Figures 3 and 4 show HRSTEM images of two types of edge TDs. According to our observations, these dislocations are composed of two edge TDs and not just one as inferred from the cross sectional analysis above. The distance between them (0.5–1.5 nm) is too small to be identified by the conventional

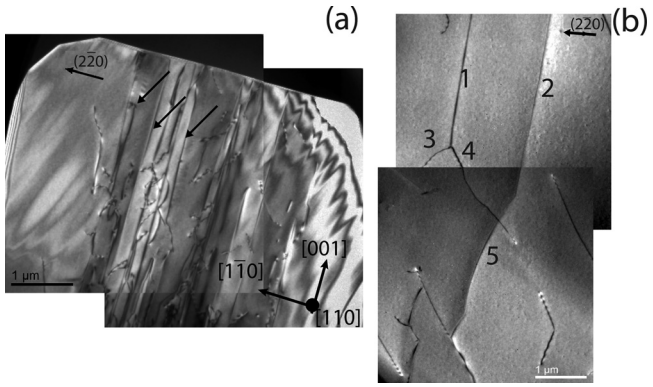

FIG. 2. Cross-sectional DF images of a Ge pillar under $\vec{g} = (2\bar{2}0)$ diffraction condition: (a) top of a Ge pillar showing edge TDs (black arrows) and (b) formation of the edge TDS.

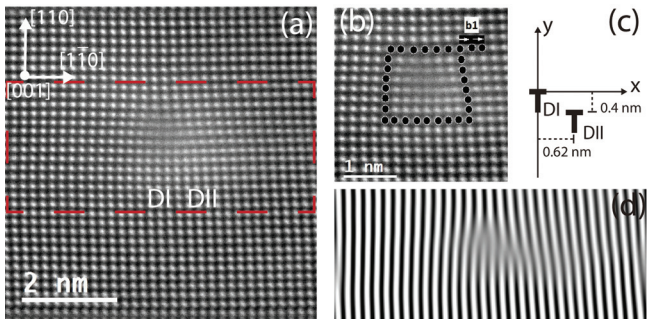

FIG. 3. Parallel edge TDs with the Burgers vector $\vec{b} = \frac{1}{2}\langle 1\bar{1}0\rangle$: (a) Plan-view HAADF-STEM image, (b) Burgers circuit around the dislocations, (c) scheme of the dislocation geometry (x and y), and (d) Moire pattern using the $(2\bar{2}0)$ reflection.

dislocation analysis. These kind of dislocations are always present in the Ge crystals as two parallel edge TDs (indicated as *DI* and *DII* in Figs. 3(a) and 4(b)) with the same ($B||$) or perpendicular ($B\perp$) Burgers vector $\vec{b} = \frac{1}{2}\langle 110\rangle$ and the same magnitude. Figure 3(d) shows the Moire pattern extracted from the red area outlined in Fig. 3(a) and obtained using the $(2\bar{2}0)$ reflection from the type $B||$ dislocations. The half planes are located at $(2\bar{2}0)$ planes separated by 0.62 nm and they lie in parallel (220) slip planes with a separation of 0.4 nm (Fig. 3(c)). Figure 3(b) shows the Burgers circuit around the TDs according to the convention start-finish;[20] the vector for closing the circuit is $\vec{b} = \frac{1}{2}[1\bar{1}0]$ for both dislocations confirming the $\vec{g}.\vec{b} = 0$ analysis. In order to determine the behavior of the dislocations, the interaction force between them was examined. Thus, the interaction of two dislocations lying in different slip planes (Figure 3(c)) with the same Burgers vector is given by the component force (F) along the x direction ($F_x = \frac{Gb^2}{2\pi(1-\nu)}\frac{x(x^2-y^2)}{x^2+y^2}$)[21] in the isotropic theory. The behavior of the dislocations is given by the variation of F_x with x, which reveals a repulsive nature since the F_x is negative in the range of x between $-0.4 < 0.65 < \infty$ ($-y < x < \infty$).[21] With the identification of the two parallel TDs, we can conclude that both 60° TDs 3 and 4 from Figure 2(b) change direction forming the parallel edge TDs ($B||$) with the same $\vec{b} = \frac{1}{2}[1\bar{1}0]$.

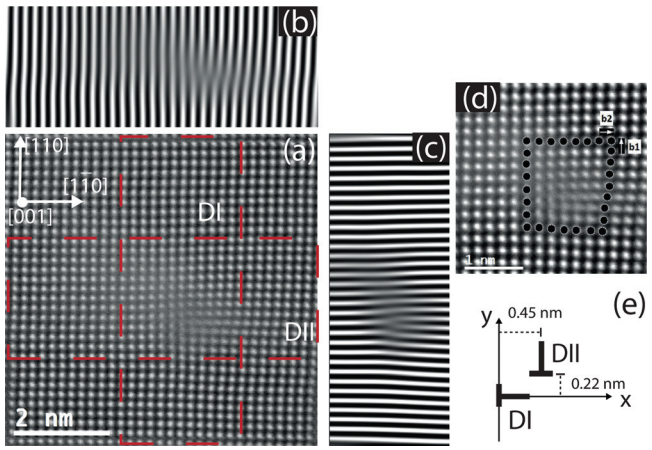

FIG. 4. Parallel edge TDs with perpendicular Burgers vector $\vec{b} = \frac{1}{2}\langle 110\rangle$: (a) Plan-view HAADF-STEM image, (b) and (c) Moire patterns using the $(2\bar{2}0)$ and (220) reflections, (d) Burgers circuit around the TDs, and (e) scheme of the dislocation geometry (x and y).

Figure 4(a) shows a HRSTEM image of the parallel edge TDs of the type $B\perp$. The Moire patterns obtained using the $(2\bar{2}0)$ and (220) reflections are shown in Figures 4(b) and 4(c). They correspond to the areas marked in red in Figure 4(a). The half planes from the two dislocations are located in perpendicular planes. The Burgers circuit of the two parallel dislocations is shown in Figure 4(d) resulting in $\vec{b} = \frac{1}{2}[110]$ and $\vec{b} = \frac{1}{2}[1\bar{1}0]$. The $\vec{g}.\vec{b} = 0$ analysis results in only $\vec{b} = \frac{1}{2}[1\bar{1}0]$, because the dislocation with $\vec{b} = \frac{1}{2}[110]$ lies on a (220) plane which is perpendicular to $(2\bar{2}0)$ and out of contrast. These dislocations cannot interact with each other because there is no energy reduction ($\frac{1}{2}[1\bar{1}0] + \frac{1}{2}[110] \rightarrow [100]$, $a^2 = a^2$).

In order to obtain the strain field interaction between the two different systems of parallel dislocations (Figs. 3(a) and 4(a)), strain analysis by the GPA method was applied to the experimental HRSTEM images (Fig. 5). The phase images used for the strain analysis were obtained by selecting the (220) and $(2\bar{2}0)$ reflections from the power spectrum. Figures 5(a) and 5(c) show the images of the experimental ε_{xx} and ε_{xy} strain fields from the $B||$ and $B\perp$ TDs, respectively. The color scale indicates that the strain ranges from −20% to 20%. The largest strain is found close to the core, while the strain decays with the distance from the core. The strain fields show that in the core of the TDs the compressive region has negative values due to the extra half plane, whereas positive values are in the tensile region. Two parallel dislocations with the same Burgers vectors in the same plane will repel each other due to the same negative or positive regions; the same happens when the dislocations are in different parallel slip planes. According to the configuration

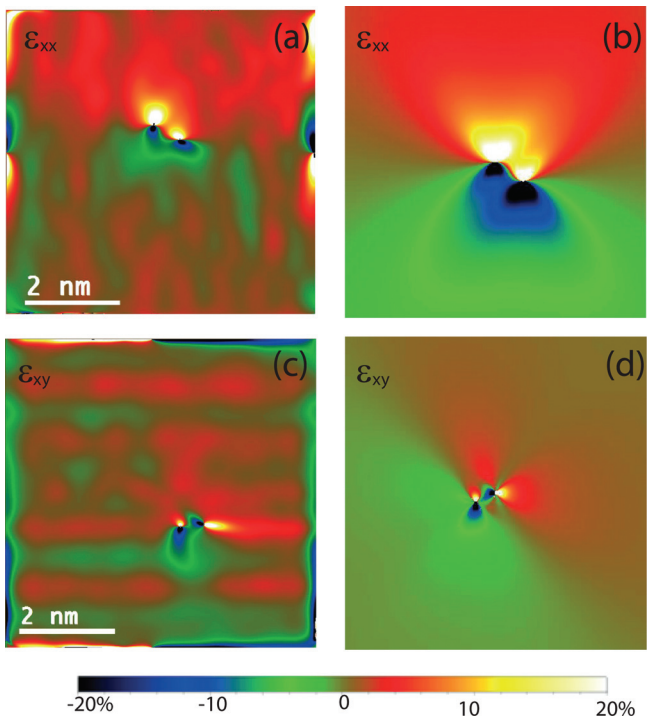

FIG. 5. Strain fields of the two dislocation systems (with $B||$ and $B\perp$): (a) experimental ε_{xx} from $B||$, (b) simulated ε_{xx} from $B||$, (c) experimental ε_{xy} from $B\perp$, and (d) simulated ε_{xy} from $B\perp$.

of the $B||$ dislocations in Fig. 5(a), the tensile region from DII is attracted by the compressive region of DI resulting in a partial annihilation of the strain fields. This means that the tensile region is smaller in DII than in DI and the compressive region of DI is smaller than in DII. Therefore, the strain field of DII is affected by the strain field of DI. The behavior of the parallel TDs with $B\perp$ is different from that of $B||$. According to the configuration of $B\perp$, the strain fields interact more strongly reducing the compressive and tensile regions as can be observed in Figure 5(c). The tensile region of DI is attracted by the compressive region of DII resulting in a partial annihilation of the strain field in this area, and the compressive region of DII is repelled by the compressive region of DI.

Strain maps were calculated using the anisotropic elastic theory (Figure 5(b) and 5(d)), where the strain field was calculated by the numerical differentiation of the displacements u_x and u_y ($\varepsilon_{xx} = (\frac{\partial u_x}{\partial x})$, $\varepsilon_{xy} = \frac{1}{2}(\frac{\partial u_x}{\partial y} + \frac{\partial u_y}{\partial x})$). For the $B||$ dislocation system, the strain fields show a butterfly shape, which match well with the experimental one. For the $B\perp$ TDs, the simulated image has an excellent fit with the experimental one, showing negatives values of the interaction force also in this case. Therefore, the anisotropic elastic theory for straight dislocations fits very well to the two types of parallel dislocations. Often, the Peierls-Nabarrow model is used to describe the strain field of the core of dislocations and yields a good match between experiments and simulations. In our case, it is not possible to use the Peierls-Nabarrow model because it is a one dimension model (with the displacement along the x_1 direction). The $B\perp$ dislocation system consists of two parallel dislocations with perpendicular Burgers vectors with displacements along x and y; therefore, a two dimension model is needed.

In summary, the edge TDs are created by a change of direction of 60° or dislocation loops. They consists of two closely spaced parallel dislocations with either equivalent or perpendicular Burgers vector $\vec{b} = \frac{1}{2}\langle 110\rangle$. Our observations show that partial annihilation of the strain fields takes place for both dislocations systems. The simulation of the strain fields using the anisotropic elastic theory confirms the experimental results.

Financial support by the Sinergia project NOVIPIX of the Swiss National Science Foundation and ETH Research Grant No. ETH-2011-2 and access to the FIB sample preparation at the Scientific Center for Optical and Electron Microscopy (ScopeM) of ETHZ are acknowledged. We also thank C. V. Falub for fruitful discussions and SEM pictures.

[1]S. Mahajan, Acta Mater. **48**, 137 (2000).
[2]D. Paul, Semicond. Sci. Technol. **19**, R75 (2004).
[3]E. Fitzgerald, Y.-H. Xie, M. Green, D. Brasen, A. Kortan, J. Michel, Y.-J. Mii, and B. Weir, Appl. Phys. Lett. **59**, 811 (1991).
[4]D. Blavette, E. Cadel, A. Fraczkiewicz, and A. Menand, Science **286**, 2317 (1999).
[5]L. M. Giovane, H.-C. Luan, A. M. Agarwal, and L. C. Kimerling, Appl. Phys. Lett. **78**, 541 (2001).
[6]A. Marzegalli, M. Brunetto, M. Salvalaglio, F. Montalenti, G. Nicotra, M. Scuderi, C. Spinella, M. De Seta, and G. Capellini, Phys. Rev. B **88**, 165418 (2013).
[7]A. Marzegalli, F. Isa, H. Groiss, E. Mueller, C. Falub, A. Taboada, P. Niedermann, G. Isella, F. Schaeffler, F. Montalenti, H. von Kaenel, and L. Miglio, Adv. Mater. **25**, 4408 (2013).
[8]H. Groiss, M. Glaser, A. Marzegalli, F. Isa, G. Isella, L. Miglio, and F. Schaeffler, Microsc. Microanal. **3**, 637 (2015).
[9]S. Harada, J. Kikkawa, Y. Nakamura, G. Wang, M. Caymax, and A. Sakai, Thin Solid Films **520**, 3245 (2012).
[10]C. Falub, H. von Kaenel, F. Isa, R. Bergamaschini, A. Marzegalli, D. Chrastina, G. Isella, E. Mueller, P. Niedermann, and L. Miglio, Science **335**, 1330 (2012).
[11]M. Couillard, G. Radtke, and G. Botton, Philos. Mag. **93**, 1250 (2013).
[12]C. Zhao, Y. Xing, C. Zhou, and P. Bai, Acta Mater. **56**, 2570 (2008).
[13]Q. Liu, C. Zhao, S. Su, J. Li, Y. Xing, and B. Cheng, PLoS One **8**, e62672 (2013).
[14]Y. Wang, X. Liu, and G. Qin, Micron **69**, 21 (2015).
[15]Q. Liu, C. Zhao, Y. Xing, S. Su, and B. Cheng, Opt. Lasers Eng. **50**, 796 (2012).
[16]M. Hytch, E. Snoeck, and R. Kilaas, Ultramicroscopy **74**, 131 (1998).
[17]Y. Guo, J. Wang, Z. Wang, J. Li, S. Tang, F. Liu, and Y. Zhou, Philos. Mag. **95**, 973 (2015).
[18]F. Montalenti, M. Salvalaglio, A. Marzegalli, P. Zaumseil, G. Capellini, T. Schuelli, M. Schubert, Y. Yamamoto, B. Tillack, and T. Schroeder, Phys. Rev. B **89**, 014101 (2014).
[19]J. Li, C. Zhao, Y. Xing, S. Su, and B. Cheng, Materials **6**, 2130 (2013).
[20]J. P. Hirth and J. Lothe, *Theory of Dislocations* (Krieger, 1992).
[21]D. Hull and D. J. Bacon, *Introduction to Dislocations* (Butterworth-Heinemann, 2011).